Journal Pre-proofs

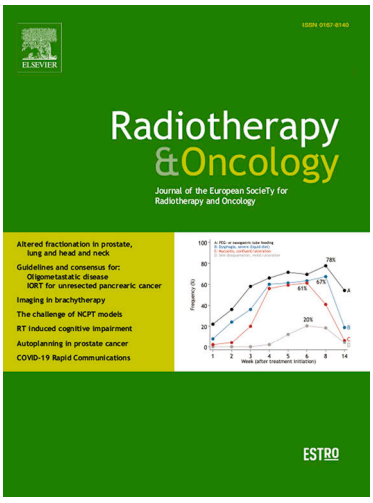

Review Article

The role of computational methods for automating and improving clinical target volume definition

Jan Unkelbach, Thomas Bortfeld, Carlos E. Cardenas, Vincent Gregoire, Wille Hager, Ben Heijmen, Robert Jeraj, Stine S Korreman, Roman Ludwig, Bertrand Pouymayou, Nadya Shusharina, Jonas Söderberg, Iuliana Toma-Dasu, Esther G.C. Troost, Eliana Vasquez Osorio

PII: S0167-8140(20)30838-0
DOI: https://doi.org/10.1016/j.radonc.2020.10.002
Reference: RADION 8568

To appear in: *Radiotherapy and Oncology*

Received Date: 10 July 2020
Revised Date: 1 October 2020
Accepted Date: 1 October 2020

Please cite this article as: Unkelbach, J., Bortfeld, T., Cardenas, C.E., Gregoire, V., Hager, W., Heijmen, B., Jeraj, R., Korreman, S.S., Ludwig, R., Pouymayou, B., Shusharina, N., Söderberg, J., Toma-Dasu, I., Troost, E.G.C., Vasquez Osorio, E., The role of computational methods for automating and improving clinical target volume definition, *Radiotherapy and Oncology* (2020), doi: https://doi.org/10.1016/j.radonc.2020.10.002

Title:

The role of computational methods for automating and improving clinical target volume definition

First and Corresponding author:

Jan Unkelbach,
Department of Radiation Oncology,
University Hospital Zurich,
Ramistrasse 100,
8091 Zurich,
Switzerland,
jan.unkelbach@usz.ch

Coauthors:

Thomas Bortfeld, Division of Radiation Biophysics, Massachusetts General Hospital and Harvard Medical School, Boston, MA USA

Carlos E. Cardenas, Department of Radiation Physics, The University of Texas MD Anderson Cancer Center, Houston, TX USA

Vincent Gregoire, Radiation Oncology Dept. Centre Léon Bérard, Lyon, France

Wille Hager, Department of Physics, Medical Radiation Physics, Stockholm University and Department of Oncology and Pathology, Medical Radiation Physics, Karolinska Institutet, Stockholm, Sweden

Ben Heijmen, Department of Radiation Oncology, Erasmus University Medical Center (Erasmus MC), Rotterdam, The Netherlands

Robert Jeraj, Department of Medical Physics, University of Wisconsin, Madison, WI, USA

Stine S Korreman, Department of Oncology and Danish Center for Particle Therapy, Aarhus University Hospital, Department of Clinical Medicine, Aarhus University, Aarhus, Denmark

Roman Ludwig, Department of Radiation Oncology, University Hospital Zurich, Zurich, Switzerland

Bertrand Pouymayou, Department of Radiation Oncology, University Hospital Zurich, Zurich, Switzerland

Nadya Shusharina, Division of Radiation Biophysics, Massachusetts General Hospital and Harvard Medical School, Boston, MA USA

Jonas Söderberg, RaySearch Laboratories, Stockholm, Sweden

Iuliana Toma-Dasu, Department of Physics, Medical Radiation Physics, Stockholm University and Department of Oncology and Pathology, Medical Radiation Physics, Karolinska Institutet, Stockholm, Sweden

Esther G.C. Troost, Dept. of Radiotherapy and Radiation Oncology, Faculty of Medicine and University Hospital Carl Gustav Carus, Technische Universität Dresden, Dresden, Germany; OncoRay – National Center for Radiation Research in Oncology, Dresden, Germany and Helmholtz-Zentrum Dresden – Rossendorf, Institute of Radiooncology - OncoRay, Dresden, Germany.

Eliana Vasquez Osorio, Division of Cancer Sciences, Faculty of Biology, Medicine and Health, The University of Manchester

Title:

The role of computational methods for automating and improving clinical target volume definition

Abstract:

Treatment planning in radiotherapy distinguishes three target volume concepts: the gross tumor volume (GTV), the clinical target volume (CTV), and the planning target volume (PTV). Over time, GTV definition and PTV margins have improved through the development of novel imaging techniques and better image guidance, respectively. CTV definition is sometimes considered the weakest element in the planning process. CTV definition is particularly complex since the extension of microscopic disease cannot be seen using currently available in-vivo imaging techniques. Instead, CTV definition has to incorporate knowledge of the patterns of tumor progression. While CTV delineation has largely been considered the domain of radiation oncologists, this paper, arising from a 2019 ESTRO Physics research workshop, discusses the contributions that medical physics and computer science can make by developing computational methods to support CTV definition. First, we overview the role of image segmentation algorithms, which may in part automate CTV delineation through segmentation of lymph node stations or normal tissues representing anatomical boundaries of microscopic tumor progression. The recent success of deep convolutional neural networks has also enabled learning entire CTV delineations from examples. Second, we discuss the use of mathematical models of tumor progression for CTV definition, using as example the application of glioma growth models to facilitate GTV-to-CTV expansion for glioblastoma that is consistent with neuroanatomy. We further consider statistical machine learning models to quantify lymphatic metastatic progression of tumors, which may eventually improve elective CTV definition. Lastly, we discuss approaches to incorporate uncertainty in CTV definition into

treatment plan optimization as well as general limitations of the CTV concept in the case of infiltrating tumors without natural boundaries.

1. Introduction

Treatment planning in radiotherapy distinguishes three target volume concepts: GTV, CTV, and PTV. The gross tumor volume (GTV) represents the macroscopic tumor mass, which is typically detectable using biomedical imaging techniques such as computed tomography (CT), magnetic resonance imaging (MRI), and/or positron emission tomography (PET). The clinical target volume (CTV) includes microscopic extensions of the tumor in the surrounding tissue, which are not detectable with current in-vivo imaging techniques. The planning target volume (PTV) is an extension of the CTV to account for geometric uncertainty in treatment planning and delivery [1], [2].

Over the past decades, radiotherapy has seen substantial improvements in GTV and PTV definition. GTV definition has improved through the development of novel imaging techniques such as functional MRI and PET imaging. For example, FDG-PET became established for target volume definition in lung and head & neck cancer [3]. Modern image guidance using cone beam CT and more recently MRI has improved the precision in treatment delivery and has led to smaller PTV margins [4]–[8]. CTV volumes have become more standardized, e.g. through precise definitions of lymph node stations. Nevertheless, target volume definition, and especially CTV definition, is often considered the weakest link in modern precision radiotherapy [9], [10]. This becomes apparent in studies assessing the variability in target volume definition between institutions [10]–[13], which have for example been performed for head and neck cancer. Using the latest technologies such as intensity modulation and image guidance, we are thus in the paradoxical situation that we can treat lesions with millimeter precision, but the uncertainties about what should be treated can be in the order of centimeters.

CTV definition is particularly complex since the extension of microscopic disease is not visible using currently available in-vivo imaging techniques. Consequently, CTV delineation does not amount to an image segmentation task, i.e. unlike GTV definition, it does not only amount to delineating an abnormal appearing mass in CT, MR, or PET images. Instead, CTV definition has to incorporate knowledge of the patterns of tumor progression. Future progress in biomedical imaging may potentially shift the boundary between visible and invisible, i.e. between GTV and CTV. For example, better imaging may increase the sensitivity and specificity for detecting small lymph node metastases [14]. However, it is not expected that the full extent of microscopic disease will become detectable in-vivo.

While understanding microscopic tumor progression generally requires an interdisciplinary effort involving radiation oncologists, radiologists, pathologists and surgeons, there is a role for medical physicists and computer scientists in CTV definition. Computational methods can contribute to CTV delineation with different scopes:

Automation: Although CTV definition is complex, it is in practice usually based on guidelines. These guidelines can in part be followed through automated workflows to streamline the planning process and reduce the time required for manual contouring. Examples include automatic segmentation of lymph node stations for nodal CTV delineation, and automatic segmentation of normal tissues that are anatomical barriers to microscopic tumor progression such as the dura and ventricles in the case of gliomas.

Consistency: Computational methods for CTV delineation may yield more consistent target volumes, even if they are based on the same rules as current clinical guidelines, reducing human induced variability. An example is GTV-to-CTV expansion for glioblastoma, where it can be difficult to consistently account for 3D neuroanatomy in manual delineation, e.g. respecting the falx as anatomical barrier while accounting for contralateral tumor progression through the corpus callosum.

Improvement: The ultimate goal is to improve CTV definition through computational methods in the sense that a better trade-off is achieved between minimizing the risk of undertreating microscopic disease versus unnecessary exposure of normal tissues. In that sense, improvement implies some change in target volume definition compared to current practice. For example, this could be based on novel statistical or mechanistic models of locoregional tumor progression or based on improved patterns of failure analysis. An example could be personalization of elective nodal CTVs based on an individual patient's risk of microscopic involvement of lymph node stations.

This paper discusses the role of medical physics, computer science, mathematics and related disciplines for supporting CTV definition through computation methods. The paper results from a 2019 ESTRO physics workshop and its content is based on the work presented and discussed by the authors. However, closely related work from the literature has been included. The main goal of the paper is to illustrate how a variety of methodologies including image segmentation algorithms, deep learning, reaction diffusion equations, shortest path algorithms, or bayesian networks can be used to address different aspects of CTV definition. We hope that this paper inspires further work within the medical physics community on the important but arguably understudied topic of CTV definition. Section 2 provides a short summary of the foundations and general principles of CTV definition. Section 3 defines the role of automatic image segmentation algorithms for CTV definition. Section 4 discusses work on the use of mathematical models of tumor progression. Finally, Section 5 considers limitations of a binary CTV concept with a fixed prescription dose in the context of infiltrative

tumors without boundary and in the context of uncertainty in tumor extension. Initial approaches to incorporate these aspects into treatment plan optimization for intensity-modulated radiotherapy techniques are discussed.

2. Basic concepts of CTV definition

The concept of the CTV was introduced by the International Commission on Radiation Units and Measurements (ICRU) in its report 50 published in 1993 [15]. It was defined as the volume encompassing the visible and/or palpable tumor, i.e. the GTV, and the volume of surrounding normal tissues suspected of sub-clinical microscopic tumor infiltration with a given probability of occurrence considered relevant for therapy. Generally, tumor infiltration to surrounding tissues is a characteristic of malignant tumors. Per definition, benign tumors do not bear any risk of local or regional microscopic infiltration; there is thus no CTV associated with these tumors. For malignant tumors, one can generally distinguish two components of the CTV.

1. The primary tumor CTV (CTV-T), which contains tissues surrounding the primary tumor GTV (GTV-T) that are at risk of sub-clinical microscopic tumor infiltration.
2. The regional lymph node CTV (CTV-N), which contains parts of the regional lymph drainage region that is at risk of harboring occult lymph node metastases.

While the primary tumor CTV is applicable to all treatment sites, there is no lymphatic drainage of brain tumors. Thus, no regional nodal CTV is defined for brain tumors such as glioma, meningioma, or brain metastases. Many other tumors including head and neck squamous cell carcinoma (HNSCC), non-small cell lung cancer (NSCLC), and breast cancer spread through the lymphatic system and form metastases in regional lymph nodes [3].

In the case of definitive radiotherapy, the primary tumor CTV contains the primary tumor GTV. If applicable, the nodal CTV contains the nodal GTV (GTV-N), i.e. macroscopic lymph node metastases usually detected through PET-CT imaging. For adjuvant radiotherapy following surgical resection of the primary tumor and/or nodal regions, the CTV often contains the surgical cavity plus unresected tissues at risk of microscopic tumor infiltration.

There are mainly three sources of data that inform CTV definition. First, histopathological examination of tissue after resection. Such data usually require surgical resection of the tumor and the surrounding tissue and is therefore difficult to obtain for tumor sites treated definitively with radiotherapy. Second, imaging data for cohorts of patients. Even though imaging data does not show the extent of microscopic tumor for any individual patient, it does inform about the general patterns of tumor progression. Third, patterns of failure

analysis, i.e. analysis of the location of tumor recurrences. One role of computational methods is to provide improved quantitative analysis of these data.

2.1. Primary tumor CTV

Distinct tumor sites differ strongly regarding their characteristics of infiltrating surrounding tissues. First, tumor sites differ by how far they infiltrate normal tissues beyond the visible GTV, ranging from a few mm to several cm. Second, tumor sites differ in their spatial complexity of microscopic spread. While some tumors show approximately isotropic infiltration around the GTV, others show preferred directions of progression and consequently anisotropic GTV-to-CTV expansion. Microscopic spread may be constrained by tissues that represent anatomical barriers for migrating tumor cells. In addition, tumors may spread anisotropically because tumor cells preferentially migrate within the tissue they arise from, or because this tissue has an inherently anisotropic structure. Gliomas are an example for the latter. For such sites, manual contouring of the CTV may be challenging and time-consuming and they are thus an interesting target for developing computational methods (see section 4.1). A short summary of tumor infiltration patterns of different tumors is provided in section S2.1 in the supplementary materials.

2.2. Regional lymph node CTV

The delineation of the CTV-N is based on the concept of lymph node stations, also referred to as lymph node levels in the case of HNSCC. Lymph node stations are anatomically defined regions of the lymph drainage system, containing the tissue surrounding lymph vessels and lymph nodes. For example, Gregoire et al. [16] provide an atlas with exact definitions of lymph node levels in the neck based on anatomical landmarks visible on CT imaging. Definition of nodal target volumes for head and neck cancer is illustrated in Figure 1. Similar atlases exist for other cancer sites [17] including breast cancer [18] and pelvic tumors [19].

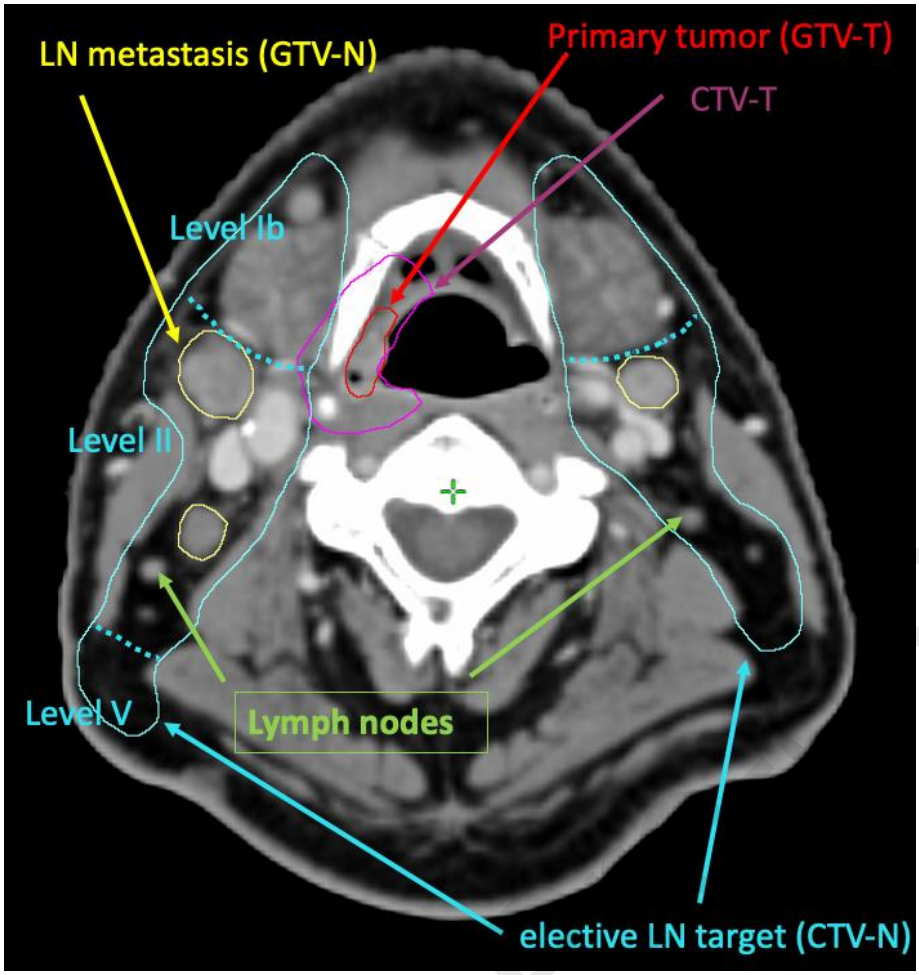

Figure 1: Illustration of target volume definition for head & neck cancer. Primary tumor GTV-T (red) and primary tumor CTV-T (purple). Suspicious enlarged lymph nodes that are assumed to harbor metastases are contoured in yellow (GTV-N). In addition, the CT image shows normal appearing lymph nodes, which may however harbor occult metastases. The nodal CTV-N is contoured in blue, containing (on this axial slice) levels Ib, II, and V ipsilaterally and levels Ib and II contralaterally.

The concept of lymph node stations subdivides the lymph drainage system into standardized volumes but does not yet define the CTV. The CTV-N is usually defined as a subset of lymph node stations, i.e. requires a decision which lymph node stations to include in the CTV-N. For some treatment sites such as NSCLC, the clinical practice moves towards only including those lymph node stations into the CTV-N that contain proven metastases. For other sites such as HNSCC, the CTV-N also contains lymph node levels that are not grossly involved, which is referred to as elective lymph node irradiation. Recommendations have been published on the selection and delineation of nodal target CTV for various primary tumor sites [16], [18], [20]–[24].

The risk of regional lymph node infiltration depends on the location and the histopathology of primary tumors. Section 4.2 discusses recent work to further personalize risk estimation of microscopic lymph node involvement based on the individual patient's state of lymphatic progression. In addition, lymphoscintigraphy has been proposed as an additional diagnostic imaging modality to assess the patient's state of nodal progression. This concept has been validated for the surgical management of regional lymph nodes in oral cavity HNSCC, melanoma, breast, prostate, and gynecological tumors, but it needs further validation studies for target volume selection in radiotherapy [25]–[30]. Moreover, the question to what level of radiation dose elective nodal target volumes must be treated warrants further investigation. For HNSCC, the elective CTV is usually treated to a uniform dose of approximately 50 Gy in 2 Gy fractions. Van den Bosch et al [31] investigate the possibility of dose de-escalation to unsuspicious lymph node levels.

3. The role of automatic image segmentation

Along with image registration, segmentation of medical images has been one of the key problems in medical image processing for several decades. In the context of radiotherapy treatment planning, image segmentation has mainly focused on organs at risk and on the GTV. These image segmentation tasks have been addressed with a variety of traditional techniques such as atlas-based segmentation or region-based methods. Such methods have been available in commercial treatment planning systems for a long time. Recently, use of neural networks, specifically deep convolutional neural networks (CNNs), have shown tremendous promise in the domain of image processing and automatic segmentation [32], with high accuracy and reduced processing time when compared with previously widely used atlas-based segmentation methods [33], [34].

Segmentation of the GTV is supported in commercial treatment planning systems via relatively simple traditional techniques such as thresholding and region growing methods. Fully automatic GTV segmentation had limited use in clinical practice so far, but had attracted significant research attention [35]–[38], which is also reflected in numerous challenges organized at Medical image computing and computed assisted intervention (MICCAI) conferences. Studies have investigated various clinical sites and combinations of imaging modalities, and performance is generally acceptable but with some systematic issues (such as inflammation related PET signal causing false positives, difficulty in detection of very small targets), and severe outliers for complex targets, which is illustrated in figure 2. This is for instance illustrated in the 2019 MICCAI Structure Segmentation Challenge where head and neck cancer and lung cancer GTVs were detected in PET-CT scans (http://www.structseg-challenge.org/#/).

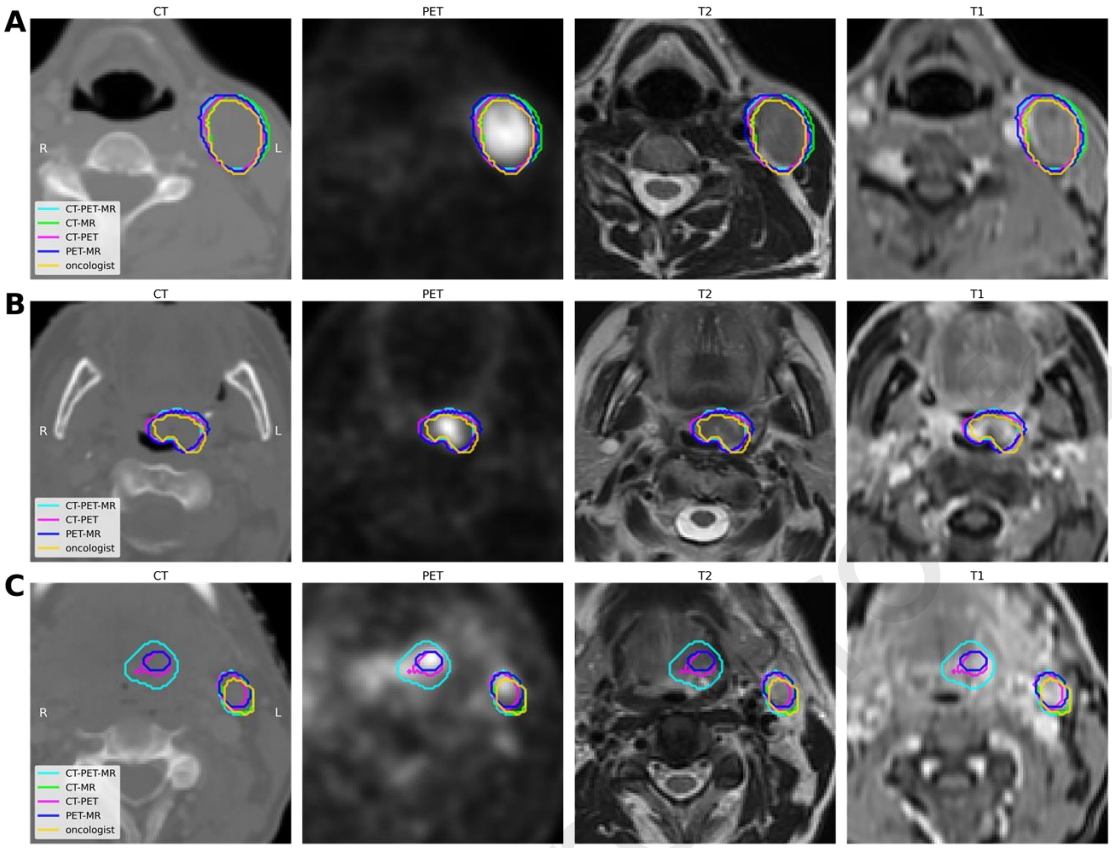

Figure 2: Three patient examples of GTV segmentation in oropharyngeal cancer using a 3D U-net network [34], based on different combinations of imaging modalities. Top row: A large lymph node target is well identified by all combinations of imaging modalities. Middle row: The primary target is only identified when PET is included, but not with CT-MR only. Bottom row: All imaging combinations with PET erroneously identify (part of) a primary target at the left side base of tongue, which is excluded by the CT-MR combination. Images courtesy of Jintao Ren, Jasper Nijkamp and Stine Korreman, Aarhus University.

Unlike the GTV, the CTV does not appear abnormal on medical images, i.e. CTV delineation does not amount to segmenting an abnormal mass on volumetric images. Nevertheless, there is a substantial role for image segmentation algorithms for semi-automation or full automation of the CTV contouring process. In many cases, the boundary of the CTV is defined by normal anatomy. Consequently, auto-segmentation of normal anatomy can contribute to the CTV delineation task. This can be illustrated based on several examples.

- For some treatment sites, the CTV represents or includes an entire organ. The main example for that is localized prostate cancer where the CTV is the prostate gland and possibly the seminal vesicles. Thus, in the absence of extra-capsular spread, automatic segmentation of the prostate means automatic CTV definition.

- For cancers with lymphatic progression, the elective nodal CTV is defined via lymph node stations. Automatically segmenting these well-defined anatomical regions thus automates one part of the CTV delineation process.
- For many tumor sites, the CTV of the primary tumor is bounded by normal tissues that represent anatomical boundaries for the microscopic progression of tumor cells. Automatic segmentation of these tissues allows for automatic correction of CTVs for anatomical barriers, e.g. automatic cropping after an isotropic GTV-to-CTV expansion.

Deep CNNs can be thought of as a method that facilitates learning image segmentations from examples. This is in contrast to traditional methods such as region growing or graph cut methods that are purely based on image intensity gradients. In that regard, deep CNNs lend themselves to CTV definition better than traditional algorithms. Deep CNN can in principle learn CTV delineations from a large enough training imaging dataset with manually contoured CTVs. Initial work is outlined below in Section 3.4.

3.1. Automatic segmentation of primary tumor CTV via whole organs

Atlas-based segmentation of prostate and pelvic lymph nodes was investigated in [39] and deemed to be clinically feasible, improving both efficiency and consistency. Deep learning-based auto-segmentation is a fairly new technique, it has been available in commercial contouring software since 2018. Deep learning has been successful for segmenting organs at risk and shows promising results for CTV delineation for prostate cancer. Auto-segmentation of the prostate from CT images with deep learning was studied in [40], with results comparable to that of manually created contours. Segmentation of prostate and seminal vesicles on MR images was studied in [41] and deemed promising for accelerating MRI-based treatment planning.

3.2. Automatic segmentation of nodal CTVs via lymph node stations

Atlas-based segmentation of lymph node levels for head and neck was studied in [42] and it was reported that it could cut the segmentation time to one third, even though manual corrections were needed. In [43], atlas-based segmentation of whole breast and nodal regions for rectal cancer was investigated. Segmentation of the whole breast and one of the three nodal regions for rectal cancer showed potential for accelerating contouring in clinical practice. A type of model-based auto-segmentation for thoracic lymph node levels was investigated in [44] with promising preliminary results, but with a need of further development.

Deep learning-based segmentation of standardized nodal regions has not been studied much. These regions are often defined by vessels, muscles, and bones surrounding the nodal region and have a more complicated shape and boundary compared to organs. There is some evidence that deep learning works well also for nodal regions. In [45], deep learning was used for auto-segmentation of CTV for nasopharyngeal cancer on planning CT images and high accuracy was reported. Given the success of deep learning for solving a large range of image analysis problems it will be interesting to see if it is suited for segmentation of nodal regions.

3.3. Segmentation of anatomical barriers of tumor infiltration

For many treatment sites, the primary tumor CTV is derived from the primary tumor GTV via a margin extension. However, these extensions often have to be corrected for anatomical barriers of tumor invasion. For example, in lung cancer, CTV-T expansions are limited to the lung tissue while the pleura and structures in the mediastinum such as vessels and airways are excluded from the CTV-T. Automatic segmentation of these structures allows for automatic correction of GTV-to-CTV expansions for anatomical barriers. In the case of lung cancer, this can simply be done by an initial isotropic expansion of the GTV-T, from which the regions that overlap with barriers are removed.

Similarly, glioblastoma are known to primarily spread within white matter while the ventricles and the dura with its extensions falx cerebri and tentorium cerebelli represent barriers for tumor cell spread. The work in [46] considers automatic GTV-to-CTV expansion for glioblastoma. In their approach, deep learning was used for auto-segmentation of anatomical barriers, which is illustrated in Figure 3a-c. These segmentations can subsequently be used to create GTV-to-CTV expansion that respect these barriers and allow for CTV definition that is consistent with neuroanatomy (see Section 4.1).

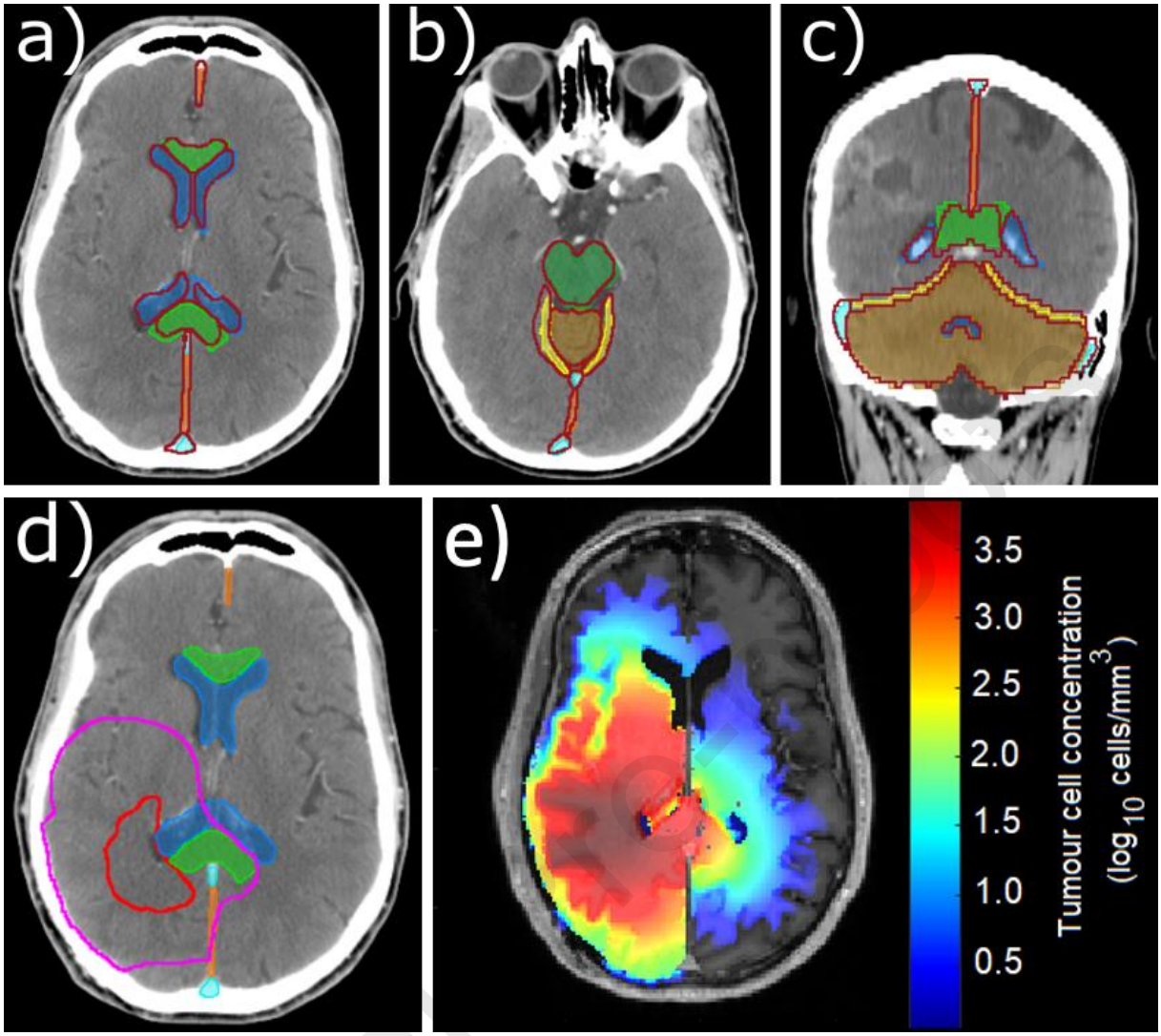

Figure 3. Example of auto-segmentation of the brain structures relevant for CTV delineation (dark red contours) in comparison with manual delineation (colored shaded structures). Two axial slices, a) and b), and one coronal slice, c), show the falx cerebri (orange), ventricles (blue), brain sinuses (cyan), corpus callosum (green), tentorium cerebelli (yellow), cerebellum (brown), and brainstem (dark green). Panel d) shows the CTV (magenta) defined as a constrained expansion of the GTV (red) by 2 cm obtained via a shortest path algorithm. Panel e) shows the tumor cell density obtained by solving the Fisher-Kolmogorov equation numerically. Unlike in panel d, reduced diffusion in grey matter was assumed.

3.4. Learning CTV delineations from examples

The segmentation problems discussed above in section 3.1. to 3.3. amount to segmentation of normal anatomy rather than tumors, which can exploit the similarity between patients. Generally, fully automatic segmentation of the entire CTV presents itself as a more challenging problem. This is because the CTV will depend on the location of the GTV, which varies from patient to patient. But at the same time, the boundary of the CTV is not

determined by abnormal image intensities. Nevertheless, deep learning approaches were recently developed to automatically delineate CTV for nasopharyngeal [47] and rectal [48] breast [49], esophageal [50], and high-level-risk and all-level-risk CTV for oropharyngeal cancer [51], [52]. Results from these early studies suggested that automatic delineation of CTVs was feasible, but yet not ready for clinical use.

Cardenas et al [53] developed a deep learning approach which was designed to mimic the clinical contouring practice for head and neck cancer CTV delineation. This work used the patient's CT image as an input to a CNN but also the segmentation of the GTV as an additional input. The model is trained on a dataset of manually contoured head & neck cancer patients that represent institutional clinical practice using high-, intermediate-, and low-risk CTVs. When ground-truth and auto-segmentations were evaluated using overlap and distance metrics, it was found that these results were within the measured inter-observer variability. A subsequent physician review of automatically delineated CTVs on an independent test set suggested that 97% of CTVs (31/32 cases) were clinically acceptable with minor or no edits required (acceptable as is (n=17), minor/stylistic edits (n=14)) [54]. To address the limitation that "one person's target volume is not everyone's target volume" [55], Cardenas et al [54] developed a convolutional neural network to automatically segment individual lymph node target volumes by grouping commonly used head and neck lymph node levels (i.e. level II-IV or Ib-V). Physician review of these target volumes showed that 93% of automatically delineated lymph node level target volumes were scored as "acceptable as is", with the remaining 7% being scored as requiring minor/stylistic edits that were considered to not impact patient outcome. This model could potentially allow a radiation oncologist to design target coverage based on individual clinical practice guidelines. Prospective evaluation will help determine the clinical utility of these models.

4. The use of mathematical models of tumor progression for CTV definition

While automatic segmentation of medical images plays an important role in automating CTV delineation as described in section 3, the problem of defining the CTV generally goes beyond image segmentation. In that regard, mathematical models for tumor progression can be applied. In this section, we demonstrate this based on two treatment sites, which have been subject to prior publications.

1. CTV definition for gliomas, where mathematical tumor growth models can be used to describe the geometrically complex infiltration of the primary tumor into the adjacent normal appearing brain tissue. This may allow for automatic GTV-to-CTV expansion that is consistent with neuroanatomy.
2. Elective CTV definition for head & neck cancer, where statistical models of lymphatic progression can support the decision which lymph node levels to include in the nodal

elective CTV - a medical decision that goes beyond the technical problem of delineating lymph node levels.

4.1. GTV-to-CTV expansion for gliomas

Glioma's complex spatial growth patterns led to the development of mathematical models aiming at reproducing them. There are several classes of models reported in the literature that can be broadly divided into two categories: the analytical or continuum models, referring to macroscopic models for the tumour growth, and the discrete or stochastic models, focussing on the extension and the cellular interplay at microscopic level. They have different underlying principles and degrees of complexity and are usually presented in conjunction with *in silico* simulations of the target and models for radiation treatment response but their clinical impact has so far been very limited [56]. One of the most frequently used mathematical approaches for describing the growth of gliomas at macroscopic level is based on a reaction-diffusion equation of Fisher–Kolmogorov type [57], [58] and accounts for the proliferation of glioma cells and the invasion in neighbouring healthy brain tissues.

$$\frac{\partial}{\partial t}c(r,t) = \nabla \cdot (\mathrm{D}(r)\nabla \mathrm{c}(r,t)) + \rho c(r,t)\left(1 - \frac{c(r,t)}{c^{\max}}\right)$$

The growth of gliomas is modelled by a partial differential equation for the variation of the tumor cell density $c(r,t)$ in space r and time t. The diffusion coefficient $\mathrm{D}(r)$ describes the motility of glioma cells through tissue while the second term represents logistic growth of glioma cells [58], [59]. The result of this approach is a time-dependent anisotropic glioma growth model. It may account for the limited motility of the glioma cells through grey matter by assuming a lower diffusion coefficient, and may model preferential invasion along the white matter fibers by incorporating DTI into the construction of $\mathrm{D}(r)$. Anatomical barriers may be modeled as no-flux boundary conditions.

Figure 3e shows a tumor cell distribution obtained from numerically solving the Fisher-Kolmogorov equation for a glioblastoma located close to the corpus callosum. Falx and ventricles are considered as boundaries for tumor infiltration while accounting for spread of tumor cells into the contralateral hemisphere via the corpus callosum. Reduced cell diffusion in grey matter was assumed, leading to lower tumor cell density near major sulci such as the lateral sulcus.

While the temporal dimension allows for modelling disease progression over time, its relevance for the definition of the CTV is rather limited. In the context of radiotherapy planning, one is interested in the anisotropic infiltration of the glioma cells in the normal tissue outside the observable border of the lesion visible on imaging, thus on the extent of the target at the time of radiotherapy treatment planning. Mathematically, the temporal component can be eliminated by assuming that, at the time of treatment planning, the

solution of the Fisher-Kolmogorov equation has reached its asymptotic solution. Asymptotically, the temporal evolution of the tumor cell density is described by a traveling wave front that moves outward from the GTV into the normal appearing brain tissue. The propagation of the tumor front can then be described through Eikonal differential equations. In order to relate the model to the patient images, the key assumption is that the boundary of GTV can be regarded as an isoline of the tumor cell density [60]. To obtain an estimate of the tumor cell density at the time of radiotherapy planning, the Eikonal equations can be solved numerical through fast marching methods [60]–[63]. Subsequently, the CTV can be defined as an isoline of the tumor cell density [60], [64].

The use of fast marching methods gives rise to an alternative interpretation of the tumor growth model. For every voxel in the brain, the Eikonal equation effectively defines a geodesic distance from the GTV contour. Here, geodesic distance means that, unlike a simple euclidean distance between voxels, a distance measure is defined that incorporates detours around anatomical barriers that tumor cells have to take when migrating from the GTV to a point in the brain.

This interpretation relates the work on the Fisher-Kolmogorov glioma growth model to the work presented by Shusharina et al [46]. The authors implemented the Dijkstra's network path algorithm [65], [66], a search for the shortest path on the voxel connectivity graph generated from a voxel grid. For a given voxel outside of the GTV, the effective distance is calculated as the sum of path length increments for the connected path from the GTV surface to that voxel. The graph edges are assigned weights corresponding to the resistance to tumor spread. The effective distance is defined as the shortest possible path. Unlike the biologically inspired Fisher-Kolmogorov model, the work by Shusharina et al is motivated geometrically and aims at automating the current clinical guidelines for GTV-to-CTV expansion, both approaches effectively lead to a very similar approach to CTV definition. Figure 3d shows the GTV-to-CTV expansion for the previously discussed glioblastoma case obtained via the shortest path algorithm.

Interestingly, the recent work on GTV-to-CTV expansion using shortest path algorithms have similarities to an early attempt to automating CTV delineation that has been presented in [67]. On each image slice, the GTV contour was represented by a polygon and expanded. The expansion was further constrained by an external "envelope" and "obstacles" to be avoided in a simple geometrical manner. This pioneering work, however, did not result in a widespread clinical application or software implementation.

4.2. Elective CTV definition for head & neck cancer

Elective CTV definition for head & neck cancer is based on the concept of lymph node levels as described in section 2. Automatic segmentation of lymph node levels as described in section 3 is therefore one component in supporting CTV definition through computational methods. However, the question which levels should be included in the elective nodal CTV is not addressed by automatic segmentation algorithms. To that end, statistical models of lymphatic tumor progression have been developed that quantitatively describe the probability of the tumor to spread along the lymphatic network. Such a model can be used to calculate the probability that lymph node levels harbor occult metastases, which may in turn guide the decision which levels to include in the elective CTV. A probability of 5-10% of microscopic involvement is a commonly considered threshold for including lymph node levels into the elective CTV.

Current guidelines on elective CTV definition are mainly based on the prevalence of lymph node metastases, i.e. the percentage of patients with a given primary tumor location who are diagnosed with lymph node metastases in the different lymph node levels [20]. However, the prevalence of lymph node metastases in a population of patients does not quantify the risk of microscopic disease in an individual patient. First, the risk of microscopic involvement in a level does not only depend on the probability of the tumor to spread to that level, but also on the sensitivity and specificity of the available imaging modalities. Second, the prevalence does not quantify how much the risk of microscopic involvement in one level depends on the presence of macroscopic metastases observed in other levels. For example, one would expect the risk of microscopic involvement in level IV to be higher for a patient who harbors macroscopic metastases in levels II and III compared to a patient with metastases only in level II. However, such a personalization of microscopic risk estimation based on a patient's individual state of lymphatic progression has not been investigated sufficiently.

Pouymayou et al [68], [69] presented a statistical model of lymphatic tumor progression in head & neck cancer using the methodology of Bayesian networks [70], which is illustrated in figure 4. In this model, each lymph node level is associated with a binary random variable for the microscopic state, which indicates whether or not the level truly harbors tumor including occult metastases. The microscopic state is a latent state that is not directly observable for radiotherapy patients. Associated with the microscopic state is an observable macroscopic state, which indicates whether a lymph node level contains visible metastases based on PET-CT imaging (and possible additional diagnostic modalities). Macroscopic and microscopic states are linked via the specificity and sensitivity of PET-CT imaging. The microscopic states are connected via directed arcs if one lymph node level receives efferent lymphatics from the other. Each arc is associated with a probability of tumors to spread from one level to the next. For example, level II and level III are connected by an arc reflecting the directional lymph flow from level II to level III, which allows tumors to spread from level II further down to level III. Thus, the graph of the Bayesian network reflects the anatomy of the lymphatic drainage system.

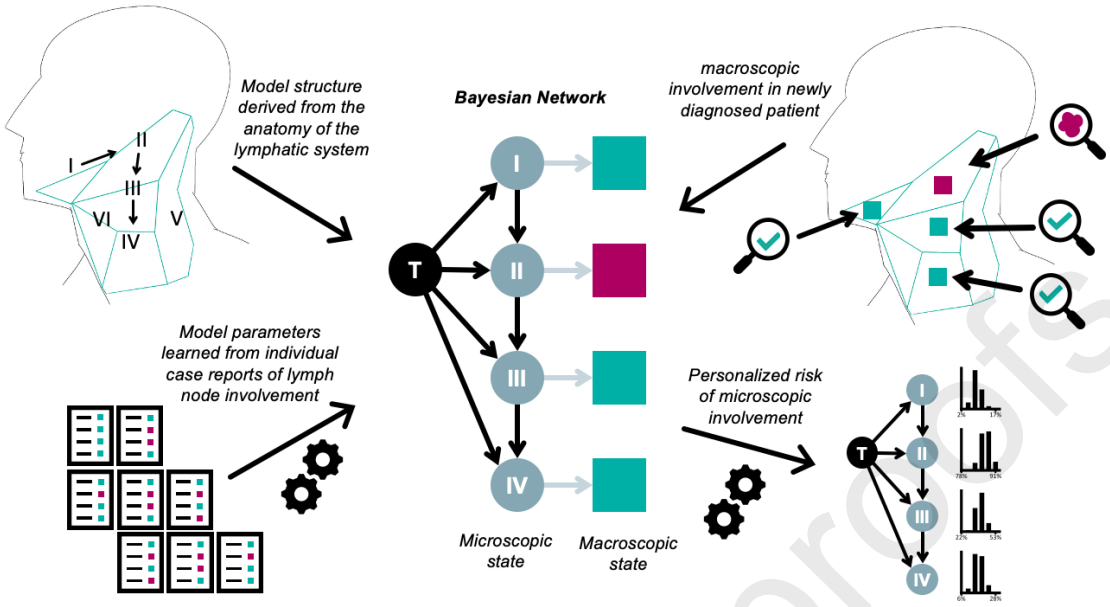

Figure 4: Illustration of a Bayesian network model for lymphatic progression of head and neck cancer. The microscopic state is depicted as round nodes, the macroscopic state (typically corresponding to PET-CT imaging) as square nodes (positive findings are illustrated as purple, negative findings as green).

The parameters of the model, the probabilities of tumor cells to spread from the primary tumor site to the lymph node levels and in between lymph node levels, can be learned from datasets of lymphatic progression patterns. However, this requires more detailed knowledge than the prevalence that is reported in publications. Instead, a dataset is needed in which the detailed configuration of lymph node involvement is known for the individual patients. Except for data published by Sanguineti et al [71] for early stage oropharynx patients, such data is not made available. Hence, changes to the current guidelines on elective CTV definition based on this model would require a multi-institutional effort to acquire larger datasets of lymphatic progression patterns.

A given model can then be used to calculate the probability of microscopic involvement for a newly diagnosed patient. In this application phase, the population based knowledge on lymphatic progression patterns is combined with the individual patient's state of disease progression, i.e. the location of visible macroscopic metastases.

5. Incorporating uncertainty in tumor extension in treatment plan optimization

In current practice, target volume concepts and dose prescriptions are binary in the sense that treatment planning simultaneously aims at covering a target volume with a prescribed

dose and at achieving a steep falloff of the dose distribution outside of the target volume. This appears to contradict the continuous nature of microscopic tumor progression and does not reflect the uncertainties in the extent of the tumor. This can be illustrated for three situations:

1. Interobserver variability in contouring. Target contours may vary between different observers due to multiple reasons. GTV contours may vary due to ambiguities in the radiological appearance of the tumor, translating in differences in CTV contours derived from GTV contours.
2. Continuous fall-off of the tumor cell density. For glioblastoma, the tumor cell density is believed to drop continuously with distance from the GTV. However, glioblastoma are often thought of as a systemic disease of the brain, i.e. tumor cells may be found at any distance from the GTV. In that sense, there is no boundary of the tumor that would naturally define the CTV contour in white matter. The size of the CTV is to some degree arbitrary and it is counterintuitive that a voxel just inside the CTV should receive a fixed prescribed dose while the dose to a voxel just outside the CTV contour should be minimized.
3. Continuously varying risk of tumor presence. For cancers with lymphatic progression, the probability to find occult metastases varies continuously over different parts of the lymph drainage region.

It is useful to distinguish between a falloff of the tumor cell density and a falloff of the probability of tumor presence with distance from the GTV, as these two distinct situations may have different implications for treatment planning. Variations in the tumor cell density may give rise to dose-painting strategies as regions of very low tumor cell density may require less dose. This situation is further discussed in section S5.1 in the supplementary materials. For variations in the probability of tumor presence, implications for dose painting are less clear. Reducing the dose in regions where the probability of tumor presence is low may mean that this region is overtreated if there is no tumor, and undertreated if there is tumor. On the other hand, delivering no dose to a region with low tumor cell density may reduce tumor control probability to almost zero. Instead, not irradiating a region that is tumor with low probability reduces tumor control probability by only a small amount. Approaches to include uncertainty in tumor extension into treatment plan optimization are discussed in section S5.2 in the supplementary materials.

6. Discussion

In current practice, CTV delineation is usually a time-consuming manual process performed by the radiation oncologist. In addition, the extent of microscopic tumor spread is often not well known. Image segmentation algorithms play a significant role in automating current

guidelines to CTV definition. This includes, auto-segmentation of whole organs for treatment sites such as prostate cancer, where an entire organ is part of the CTV. Further examples are auto-segmentation of lymph node stations for the delineation of nodal CTVs and the auto-segmentation of anatomical barriers to tumor progression that are to be excluded from the CTV. Although treatment planning systems had some support for segmentation using traditional techniques, it is now widely believed that deep CNNs substantially improve accuracy and may yield a breakthrough in the practical usefulness of auto-segmentation methods.

For most tumor sites, definition of the primary tumor CTV amounts to a margin expansion around the GTV-T. For tumor sites where this expansion is anisotropic, computational methods can help creating anisotropic margins that are consistent with anatomical barriers of tumor progression and incorporate preferred directions of tumor spread. For many treatment sites such as lung cancer, it is sufficient to segment tissues not infiltrated by the tumor and remove these from the CTV-T. With further improvements in normal tissue segmentation methods, this step can potentially be fully automatic in the future. A further improvement to anisotropic margin expansion, going beyond cropping for anatomical barriers, is the use of shortest path algorithms. These methods have been developed to facilitate GTV-to-CTV expansion for glioblastoma that is consistent with neuroanatomy.

The main scope of image segmentation algorithms lies in automation of CTV definition guidelines rather than questioning the way CTV definition is currently performed and improving on it. This is in particular the case for neural network based models that are trained on examples of CTVs manually delineated based on the current state-of-the-art. However, it can be argued that an automatic segmentation algorithm that is able to reproduce CTV definitions corresponding to best current clinical practice, may improve on less experienced radiation oncologists.

Attempts to improve on current guidelines to CTV definition through computational methods go beyond automation. Given that computational methods do not generate additional experimental or clinical data, one role for computational methods consist in developing mathematical models of tumor progression, that allow for better analysis of the available data on tumor progression patterns or patterns of failure. An example for that is the development of statistical models of lymphatic progression, which may improve our understanding of microscopic involvement risk and eventually improve on the decision which parts of the lymph drainage regions should be included in the elective CTV.

Often, the question of how to validate computational tools for CTV definition is raised. In that regard it is important to consider the scope of the respective computational tool, i.e. whether the goal is automation of current guidelines or whether the goal is to change current guidelines. In the case of automatic segmentation algorithms, validation consists in

testing how accurately an algorithm can reproduce a ground truth contour, which is typically given by a manual contour provided by one or multiple experts according to guidelines. Here, the question is not whether this contour is an appropriate CTV, but only whether the algorithm does what it is expected to do. The situation is different when the goal is to change CTV definition guidelines. In this case, models of tumor progression data may influence expert recommendations or the design of clinical studies.

Eventually, target volume definition should be seen in conjunction with dose prescription and treatment plan optimization. In the context of infiltrating tumors without boundary and uncertainties in tumor extent, the concept of binary CTV volumes with a fixed prescription dose appears counterintuitive. There are approaches to incorporate these aspects in treatment plan optimization, typically through exponential cell kill models as discussed in section 5. However, providing a quantitative relation between dose and probability or density of tumor cells is inherently problematic. This limitation is similar to the difficulties faced in dose painting inside the GTV based on functional imaging.

There are many additional aspects of CTV definition not discussed in this article. One research direction is certainly the development of novel imaging modalities that shift the boundary between visible tumor (GTV) and invisible tumor (CTV). For the example of gliomas, this includes PET tracers for amino acid metabolism [3] and MRI techniques such as diffusion tensor imaging (DTI) or 2-hydroxygluterate spectroscopy imaging in IDH-mutant gliomas [72]. In combination with advanced image analysis algorithms, this may lead to improved predictions of the extent of microscopic tumor infiltration [73], [74]. Another largely unsolved problem is CTV definition in the context of adaptive radiotherapy for shrinking tumors (section S6, supplementary materials).

In conclusion, computational methods can support CTV definition in different ways. Medical image segmentation algorithms can contribute to automating current guidelines to CTV definition. This includes the delineation of anatomically defined regions of tumor progression such as lymph node stations and the segmentation of anatomical barriers for tumor progression that are accounted for in smart GTV-to-CTV margin extensions. In addition, computational methods may improve the quantitative analysis and modeling of tumor progression patterns, which may ultimately lead to improved CTV definition guidelines.

References

[1] T. Landberg *et al.*, “Report 62,” *J. Int. Comm. Radiat. Units Meas.*, vol. os32, no. 1, p. NP-NP, Nov. 1999, doi: 10.1093/jicru/os32.1.Report62.

[2] M. Van Herk, “Errors and margins in radiotherapy,” in *Seminars in radiation oncology*, 2004, vol. 14, no. 1, pp. 52–64.

[3] A. L. Grosu and C. Nieder, *Target volume definition in radiation oncology*. Springer, 2015.

[4] G. R. Borst, J.-J. Sonke, A. Betgen, P. Remeijer, M. van Herk, and J. V. Lebesque, "Kilo-voltage cone-beam computed tomography setup measurements for lung cancer patients; first clinical results and comparison with electronic portal-imaging device," *Int. J. Radiat. Oncol. Biol. Phys.*, vol. 68, no. 2, pp. 555–561, Jun. 2007, doi: 10.1016/j.ijrobp.2007.01.014.

[5] R. Topolnjak *et al.*, "Breast patient setup error assessment: comparison of electronic portal image devices and cone-beam computed tomography matching results," *Int. J. Radiat. Oncol. Biol. Phys.*, vol. 78, no. 4, pp. 1235–1243, Nov. 2010, doi: 10.1016/j.ijrobp.2009.12.021.

[6] P. Ost, W. De Gersem, B. De Potter, V. Fonteyne, W. De Neve, and G. De Meerleer, "A comparison of the acute toxicity profile between two-dimensional and three-dimensional image-guided radiotherapy for postoperative prostate cancer," *Clin. Oncol. R. Coll. Radiol. G. B.*, vol. 23, no. 5, pp. 344–349, Jun. 2011, doi: 10.1016/j.clon.2011.01.505.

[7] D. Winkel *et al.*, "Target coverage and dose criteria based evaluation of the first clinical 1.5T MR-linac SBRT treatments of lymph node oligometastases compared with conventional CBCT-linac treatment," *Radiother. Oncol. J. Eur. Soc. Ther. Radiol. Oncol.*, vol. 146, pp. 118–125, May 2020, doi: 10.1016/j.radonc.2020.02.011.

[8] D. Winkel *et al.*, "Adaptive radiotherapy: The Elekta Unity MR-linac concept," *Clin. Transl. Radiat. Oncol.*, vol. 18, pp. 54–59, Sep. 2019, doi: 10.1016/j.ctro.2019.04.001.

[9] L. Kim, C. Wang, A. Khan, and M. Pierce, "Clinical Target Volume: The Third Front," *Int J Radiat Oncol Biol Phys*, vol. 95, no. 2, pp. 800–1, Jun. 2016, doi: 10.1016/j.ijrobp.2016.01.051.

[10] C. F. Njeh, "Tumor delineation: The weakest link in the search for accuracy in radiotherapy," *J Med Phys*, vol. 33, no. 4, pp. 136–40.

[11] R. Apolle *et al.*, "Inter-observer variability in target delineation increases during adaptive treatment of head-and-neck and lung cancer," *Acta Oncol. Stockh. Swed.*, vol. 58, no. 10, pp. 1378–1385, Oct. 2019, doi: 10.1080/0284186X.2019.1629017.

[12] T. Kruser *et al.*, "NRG brain tumor specialists consensus guidelines for glioblastoma contouring," *J. Neurooncol.*, vol. 143, no. 1, pp. 157–166, 2019.

[13] S. K. Vinod, M. G. Jameson, M. Min, and L. C. Holloway, "Uncertainties in volume delineation in radiation oncology: A systematic review and recommendations for future studies," *Radiother Oncol*, vol. 121, no. 2, pp. 169–179, 2016.

[14] N. Samolyk-Kogaczewska, E. Sierko, D. Dziemianczyk-Pakiela, K. B. Nowaszewska, M. Lukasik, and J. Reszec, "Usefulness of Hybrid PET/MRI in Clinical Evaluation of Head and Neck Cancer Patients," *Cancers*, vol. 12, no. 2, Feb. 2020, doi: 10.3390/cancers12020511.

[15] I. C. on R. Units, *Prescribing, recording, and reporting photon beam therapy*, vol. 50. International Commission on Radiation, 1993.

[16] V. Gregoire *et al.*, "Delineation of the neck node levels for head and neck tumors: a 2013 update. DAHANCA, EORTC, HKNPCSG, NCIC CTG, NCRI, RTOG, TROG consensus

guidelines," *Radiother Oncol*, vol. 110, no. 1, pp. 172–81, Jan. 2014, doi: 10.1016/j.radonc.2013.10.010.

[17] "Contouring Atlases." https://www.rtog.org/CoreLab/ContouringAtlases.aspx (accessed Jul. 08, 2020).

[18] B. V. Offersen *et al.*, "ESTRO consensus guideline on target volume delineation for elective radiation therapy of early stage breast cancer," *Radiother. Oncol. J. Eur. Soc. Ther. Radiol. Oncol.*, vol. 114, no. 1, pp. 3–10, Jan. 2015, doi: 10.1016/j.radonc.2014.11.030.

[19] V. A. Harris *et al.*, "Consensus Guidelines and Contouring Atlas for Pelvic Node Delineation in Prostate and Pelvic Node Intensity Modulated Radiation Therapy," *Int. J. Radiat. Oncol. Biol. Phys.*, vol. 92, no. 4, pp. 874–883, Jul. 2015, doi: 10.1016/j.ijrobp.2015.03.021.

[20] J. Biau *et al.*, "Selection of lymph node target volumes for definitive head and neck radiation therapy: a 2019 Update," *Radiother. Oncol. J. Eur. Soc. Ther. Radiol. Oncol.*, vol. 134, pp. 1–9, 2019, doi: 10.1016/j.radonc.2019.01.018.

[21] W. Small *et al.*, "Consensus guidelines for delineation of clinical target volume for intensity-modulated pelvic radiotherapy in postoperative treatment of endometrial and cervical cancer," *Int. J. Radiat. Oncol. Biol. Phys.*, vol. 71, no. 2, pp. 428–434, Jun. 2008, doi: 10.1016/j.ijrobp.2007.09.042.

[22] O. Matzinger *et al.*, "EORTC-ROG expert opinion: radiotherapy volume and treatment guidelines for neoadjuvant radiation of adenocarcinomas of the gastroesophageal junction and the stomach," *Radiother. Oncol. J. Eur. Soc. Ther. Radiol. Oncol.*, vol. 92, no. 2, pp. 164–175, Aug. 2009, doi: 10.1016/j.radonc.2009.03.018.

[23] V. Valentini *et al.*, "International consensus guidelines on Clinical Target Volume delineation in rectal cancer," *Radiother. Oncol. J. Eur. Soc. Ther. Radiol. Oncol.*, vol. 120, no. 2, pp. 195–201, 2016, doi: 10.1016/j.radonc.2016.07.017.

[24] U. Nestle *et al.*, "ESTRO ACROP guidelines for target volume definition in the treatment of locally advanced non-small cell lung cancer," *Radiother. Oncol. J. Eur. Soc. Ther. Radiol. Oncol.*, vol. 127, no. 1, pp. 1–5, 2018, doi: 10.1016/j.radonc.2018.02.023.

[25] F. Giammarile *et al.*, "The EANM practical guidelines for sentinel lymph node localisation in oral cavity squamous cell carcinoma," *Eur. J. Nucl. Med. Mol. Imaging*, vol. 46, no. 3, pp. 623–637, 2019, doi: 10.1007/s00259-018-4235-5.

[26] F. Giammarile *et al.*, "The EANM and SNMMI practice guideline for lymphoscintigraphy and sentinel node localization in breast cancer," *Eur. J. Nucl. Med. Mol. Imaging*, vol. 40, no. 12, pp. 1932–1947, Dec. 2013, doi: 10.1007/s00259-013-2544-2.

[27] F. Giammarile *et al.*, "The EANM clinical and technical guidelines for lymphoscintigraphy and sentinel node localization in gynaecological cancers," *Eur. J. Nucl. Med. Mol. Imaging*, vol. 41, no. 7, pp. 1463–1477, Jul. 2014, doi: 10.1007/s00259-014-2732-8.

[28] C. Bluemel *et al.*, "EANM practice guidelines for lymphoscintigraphy and sentinel lymph node biopsy in melanoma," *Eur. J. Nucl. Med. Mol. Imaging*, vol. 42, no. 11, pp. 1750–1766, Oct. 2015, doi: 10.1007/s00259-015-3135-1.

[29] U. Ganswindt *et al.*, "Optimized coverage of high-risk adjuvant lymph node areas in prostate cancer using a sentinel node-based, intensity-modulated radiation therapy technique," *Int. J. Radiat. Oncol. Biol. Phys.*, vol. 67, no. 2, pp. 347–355, Feb. 2007, doi: 10.1016/j.ijrobp.2006.08.082.

[30] U. Ganswindt *et al.*, "Intensity modulated radiotherapy for high risk prostate cancer based on sentinel node SPECT imaging for target volume definition," *BMC Cancer*, vol. 5, p. 91, Jul. 2005, doi: 10.1186/1471-2407-5-91.

[31] S. van den Bosch *et al.*, "Uniform FDG-PET guided GRAdient Dose prEscription to reduce late Radiation Toxicity (UPGRADE-RT): study protocol for a randomized clinical trial with dose reduction to the elective neck in head and neck squamous cell carcinoma," *BMC Cancer*, vol. 17, no. 1, p. 208, 21 2017, doi: 10.1186/s12885-017-3195-7.

[32] S. Nikolov *et al.*, "Deep learning to achieve clinically applicable segmentation of head and neck anatomy for radiotherapy," 2018.

[33] J. F. Daisne and A. Blumhofer, "Atlas-based automatic segmentation of head and neck organs at risk and nodal target volumes: a clinical validation," *Radiat Oncol*, vol. 8, p. 154, 2013.

[34] A. K. Hoang Duc *et al.*, "Validation of clinical acceptability of an atlas-based segmentation algorithm for the delineation of organs at risk in head and neck cancer," *Med Phys*, vol. 42, no. 9, pp. 5027–5034, 2015.

[35] B. H. Menze *et al.*, "The Multimodal Brain Tumor Image Segmentation Benchmark (BRATS)," *IEEE Trans. Med. Imaging*, vol. 34, no. 10, pp. 1993–2024, 2015.

[36] S. Pereira, A. Pinto, V. Alves, and C. A. Silva, "Brain Tumor Segmentation Using Convolutional Neural Networks in MRI Images," *IEEE Trans Med Imaging*, vol. 35, no. 5, pp. 1240–1251, 2016.

[37] Y. Zhuge *et al.*, "Brain tumor segmentation using holistically nested neural networks in MRI images," *Med Phys*, vol. 44, no. 10, pp. 5234–5243, 2017.

[38] B. Huang *et al.*, "Fully Automated Delineation of Gross Tumor Volume for Head and Neck Cancer on PET-CT Using Deep Learning: A Dual-Center Study," *Contrast Media Mol. Imaging*, p. 8923028, 2018, doi: 10.1155/2018/8923028.

[39] S. Pejavar *et al.*, "Computer-assisted, atlas-based segmentation for target volume delineation in whole pelvic IMRT for prostate cancer," *Technol. Cancer Res. Treat.*, vol. 12, no. 3, Art. no. 3, Jun. 2013, doi: 10.7785/tcrt.2012.500313.

[40] C. Liu *et al.*, "Automatic Segmentation of the Prostate on CT Images Using Deep Neural Networks (DNN)," *Int. J. Radiat. Oncol. Biol. Phys.*, vol. 104, no. 4, Art. no. 4, 15 2019, doi: 10.1016/j.ijrobp.2019.03.017.

[41] S. Elguindi *et al.*, "Deep learning-based auto-segmentation of targets and organs-at-risk for magnetic resonance imaging only planning of prostate radiotherapy," *Phys. Imaging Radiat. Oncol.*, vol. 12, pp. 80–86, Oct. 2019, doi: 10.1016/j.phro.2019.11.006.

[42] D. N. Teguh *et al.*, "Clinical Validation of Atlas-Based Auto-Segmentation of Multiple Target Volumes and Normal Tissue (Swallowing/Mastication) Structures in the Head and

Neck," *Int. J. Radiat. Oncol. Biol. Phys.*, vol. 81, no. 4, Art. no. 4, Nov. 2011, doi: 10.1016/j.ijrobp.2010.07.009.

[43] L. C. Anders, F. Stieler, K. Siebenlist, J. Schaefer, F. Lohr, and F. Wenz, "Performance of an atlas-based autosegmentation software for delineation of target volumes for radiotherapy of breast and anorectal cancer.," *Radiother. Oncol. J. Eur. Soc. Ther. Radiol. Oncol.*, 2012, doi: 10.1016/j.radonc.2011.08.043.

[44] D. Sarrut, L. Claude, S. Rit, R. Pinho, G. Pitson, and R. Lynch, "Investigating mediastinal lymph node stations segmentation on thoracic CT following experts guidelines," in *MICCAI, First International Workshop on Image-Guidance and Multimodal Dose Planning in Radiation Therapy*, Nice, France, Oct. 2012, p. 1, Accessed: Jun. 01, 2020. [Online]. Available: https://hal.archives-ouvertes.fr/hal-00838747.

[45] K. Men *et al.*, "Deep Deconvolutional Neural Network for Target Segmentation of Nasopharyngeal Cancer in Planning Computed Tomography Images," *Front. Oncol.*, vol. 7, p. 315, 2017.

[46] N. Shusharina, J. Söderberg, D. Edmunds, F. Löfman, H. Shih, and T. Bortfeld, "Automated delineation of the clinical target volume using anatomically constrained 3D expansion of the gross tumor volume," *Radiother. Oncol.*, vol. 146, pp. 37–43, 2020, doi: 10.1016/j.radonc.2020.01.028.

[47] K. Men *et al.*, "Deep Deconvolutional Neural Network for Target Segmentation of Nasopharyngeal Cancer in Planning Computed Tomography Images," *Front. Oncol.*, vol. 7, p. 315, 2017, doi: 10.3389/fonc.2017.00315.

[48] K. Men, J. Dai, and Y. Li, "Automatic segmentation of the clinical target volume and organs at risk in the planning CT for rectal cancer using deep dilated convolutional neural networks," *Med Phys*, vol. 44, no. 12, pp. 6377–6389, 2017.

[49] K. Men *et al.*, "Fully automatic and robust segmentation of the clinical target volume for radiotherapy of breast cancer using big data and deep learning," *Phys. Med.*, vol. 50, pp. 13–19, Jun. 2018, doi: 10.1016/j.ejmp.2018.05.006.

[50] D. Jin *et al.*, "Deep esophageal clinical target volume delineation using encoded 3d spatial context of tumors, lymph nodes, and organs at risk," in *International Conference on Medical Image Computing and Computer-Assisted Intervention*, 2019, pp. 603–612.

[51] C. E. Cardenas *et al.*, "Auto-delineation of oropharyngeal clinical target volumes using 3D convolutional neural networks," *Phys Med Biol*, vol. 63, no. 21, p. 215026, 2018.

[52] C. E. Cardenas *et al.*, "Deep Learning Algorithm for Auto-Delineation of High-Risk Oropharyngeal Clinical Target Volumes With Built-In Dice Similarity Coefficient Parameter Optimization Function," *Int J Radiat Oncol Biol Phys*, vol. 101, no. 2, pp. 468–478, 2018.

[53] C. Cardenas *et al.*, "Identifying Oropharyngeal Clinical Target Volumes Delineation Patterns From Peer-Reviewed Clinical Delineations Via Cascade 3D Fully-Convolutional Networks," in *MEDICAL PHYSICS*, 2019, vol. 46, no. 6, pp. E296–E296.

[54] C. E. Cardenas, B. M. Beadle, D. J. Rhee, R. McCarroll, L. Zhang, and J. Yang, "Delivering high-quality head-and-neck low-risk clinical target volumes through a fully-

automated artificial intelligence-based approach," *Int. J. Radiat. Oncol. Biol. Phys.*, vol. 106, no. 5, p. 1122, 2020.

[55] B. M. Beadle and C. M. Anderson, "CTV Guidance for Head and Neck Cancers," *Int. J. Radiat. Oncol. Biol. Phys.*, vol. 100, no. 4, pp. 903–905, 15 2018, doi: 10.1016/j.ijrobp.2017.12.264.

[56] M. Protopapa *et al.*, "Clinical implications of in silico mathematical modeling for glioblastoma: a critical review," *J. Neurooncol.*, vol. 136, no. 1, pp. 1–11, 2018.

[57] J. D. Murray, *Mathematical Biology II: Spatial Models and Biomedical Applications*. New York: Springer, 2003.

[58] H. L. P. Harpold, E. C. Alvord, and K. R. Swanson, "The evolution of mathematical modeling of glioma proliferation and invasion," *J Neuropathol. Exp Neurol*, vol. 66, no. 1, pp. 1–9, 2007.

[59] K. R. Swanson, R. C. Rostomily, and E. C. Alvord, "A mathematical modelling tool for predicting survival of individual patients following resection of glioblastoma: a proof of principle," *Br J Cancer*, vol. 98, no. 1, pp. 113–119, Jan. 2008.

[60] E. Konukoglu, O. Clatz, P. Y. Bondiau, H. Delingette, and N. Ayache, "Extrapolating glioma invasion margin in brain magnetic resonance images: suggesting new irradiation margins," *Med Image Anal*, vol. 14, no. 2, pp. 111–25, Apr. 2010, doi: 10.1016/j.media.2009.11.005.

[61] J. A. Sethian, "A fast marching level set method for monotonically advancing fronts," *Proc Natl Acad Sci USA*, vol. 93, pp. 1591–1595, 1996.

[62] J. A. Sethian, "Fast Marching Methods," *SIAM Rev.*, vol. 41, pp. 199–235, 1999.

[63] J. A. Sethian, "Evolution, Implementation, and Application of Level Set and Fast Marching Methods for Advancing Fronts," *J. Comput. Phys.*, vol. 169, pp. 503–555, 2001.

[64] J. Unkelbach *et al.*, "Radiotherapy planning for glioblastoma based on a tumor growth model: improving target volume delineation," *Phys Med Biol*, vol. 59, no. 3, pp. 747–70, Feb. 2014, doi: 10.1088/0031-9155/59/3/747.

[65] E. W. Dijkstra, "A note on two problems in connexion with graphs," *Numer. Math.*, vol. 1, no. 1, pp. 269–271, 1959.

[66] T. H. Cormen, C. E. Leiserson, R. L. Rivest, and C. Stein, *Introduction to algorithms*. MIT press, 2009.

[67] R. Belshi, D. Pontvert, J.-C. Rosenwald, and G. Gaboriaud, "Automatic three-dimensional expansion of structures applied to determination of the clinical target volume in conformal radiotherapy," *Int. J. Radiat. Oncol.*, vol. 37, no. 3, pp. 689–696, 1997.

[68] B. Pouymayou, P. Balermpas, O. Riesterer, M. Guckenberger, and J. Unkelbach, "A Bayesian network model of lymphatic tumor progression for personalized elective CTV definition in head and neck cancers," *Phys. Med. Biol.*, vol. 64, no. 16, p. 165003, 14 2019, doi: 10.1088/1361-6560/ab2a18.

[69] B. Pouymayou, C. Koechli, P. Balermpas, M. Guckenberger, and J. Unkelbach, "Analysis of lymphatic metastasis and progression patterns for clinical target volume (CTV)

definition in head and neck squamous cell carcinoma (HNSCC)," *Acta Oncol. Stockh. Swed.*, vol. 58, no. 10, pp. 1519–1522, Oct. 2019, doi: 10.1080/0284186X.2019.1643919.
[70] C. Bishop, *Pattern Recognition and Machine Learning*. Springer-Verlag New York, 2006.
[71] G. Sanguineti *et al.*, "Defining the risk of involvement for each neck nodal level in patients with early T-stage node-positive oropharyngeal carcinoma," *Int J Radiat Oncol Biol Phys*, vol. 74, no. 5, pp. 1356–64, Aug. 2009, doi: 10.1016/j.ijrobp.2008.10.018.
[72] K. Jafari-Khouzani *et al.*, "Volumetric relationship between 2-hydroxyglutarate and FLAIR hyperintensity has potential implications for radiotherapy planning of mutant IDH glioma patients," *Neuro Oncol*, vol. 18, no. 11, pp. 1569–1578, Nov. 2016, doi: 10.1093/neuonc/now100.
[73] J.-L. Yan, C. Li, A. van der Hoorn, N. R. Boonzaier, T. Matys, and S. J. Price, "A Neural Network Approach to Identify the Peritumoral Invasive Areas in Glioblastoma Patients by Using MR Radiomics," *Sci. Rep.*, vol. 10, no. 1, Art. no. 1, Jun. 2020, doi: 10.1038/s41598-020-66691-6.
[74] J. C. Peeken *et al.*, "Deep learning derived tumor infiltration maps for personalized target definition in Glioblastoma radiotherapy," *Radiother. Oncol. J. Eur. Soc. Ther. Radiol. Oncol.*, vol. 138, pp. 166–172, 2019, doi: 10.1016/j.radonc.2019.06.031.

Figure 1:
Illustration of target volume definition for head & neck cancer. Primary tumor GTV-T (red) and primary tumor CTV-T (purple). Suspicious enlarged lymph nodes that are assumed to harbor metastases are contoured in yellow (GTV-N). In addition, the CT image shows normal appearing lymph nodes, which may however harbor occult metastases. The nodal CTV-N is contoured in blue, containing (on this axial slice) levels Ib, II, and V ipsilaterally and levels Ib and II contralaterally.

Figure 2:
Three patient examples of GTV segmentation in oropharyngeal cancer using a 3D U-net network [34], based on different combinations of imaging modalities. Top row: A large lymph node target is well identified by all combinations of imaging modalities. Middle row: The primary target is only identified when PET is included, but not with CT-MR only. Bottom row: All imaging combinations with PET erroneously identify (part of) a primary target at the left

side base of tongue, which is excluded by the CT-MR combination. Images courtesy of Jintao Ren, Jasper Nijkamp and Stine Korreman, Aarhus University.

Figure 3:
Example of auto-segmentation of the brain structures relevant for CTV delineation (dark red contours) in comparison with manual delineation (colored shaded structures). Two axial slices, a) and b), and one coronal slice, c), show the falx cerebri (orange), ventricles (blue), brain sinuses (cyan), corpus callosum (green), tentorium cerebelli (yellow), cerebellum (brown), and brainstem (dark green). Panel d) shows the CTV (magenta) defined as a constrained expansion of the GTV (red) by 2 cm obtained via a shortest path algorithm. Panel e) shows the tumor cell density obtained by solving the Fisher-Kolmogorov equation numerically. Unlike in panel d, reduced diffusion in grey matter was assumed.

Figure 4:
Illustration of a Bayesian network model for lymphatic progression of head and neck cancer. The microscopic state is depicted as round nodes, the macroscopic state (typically corresponding to PET-CT imaging) as square nodes (positive findings are illustrated as purple, negative findings as green).

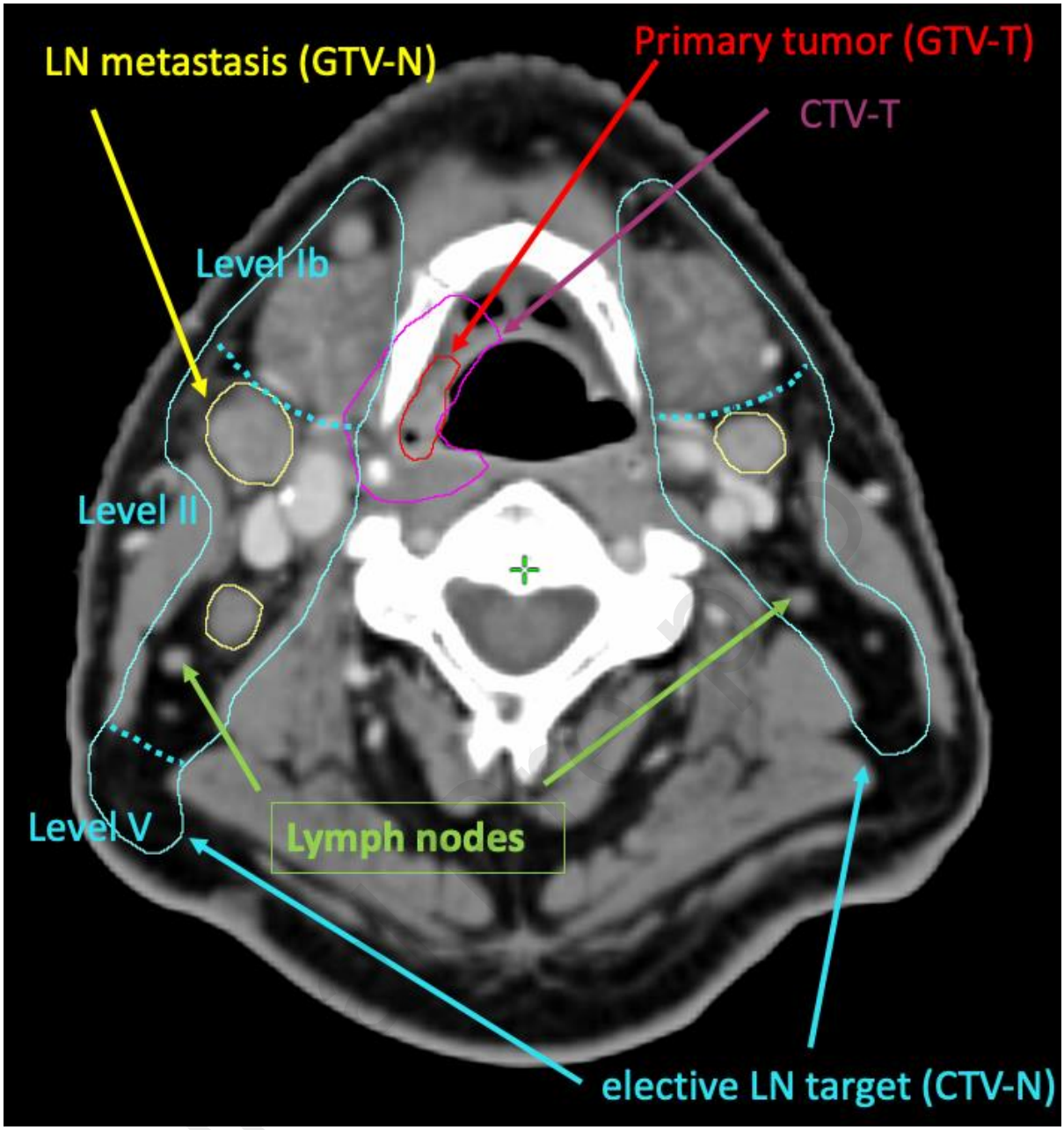
LN metastasis (GTV-N)
Primary tumor (GTV-T)
CTV-T
Level Ib
Level II
Level V
Lymph nodes
elective LN target (CTV-N)

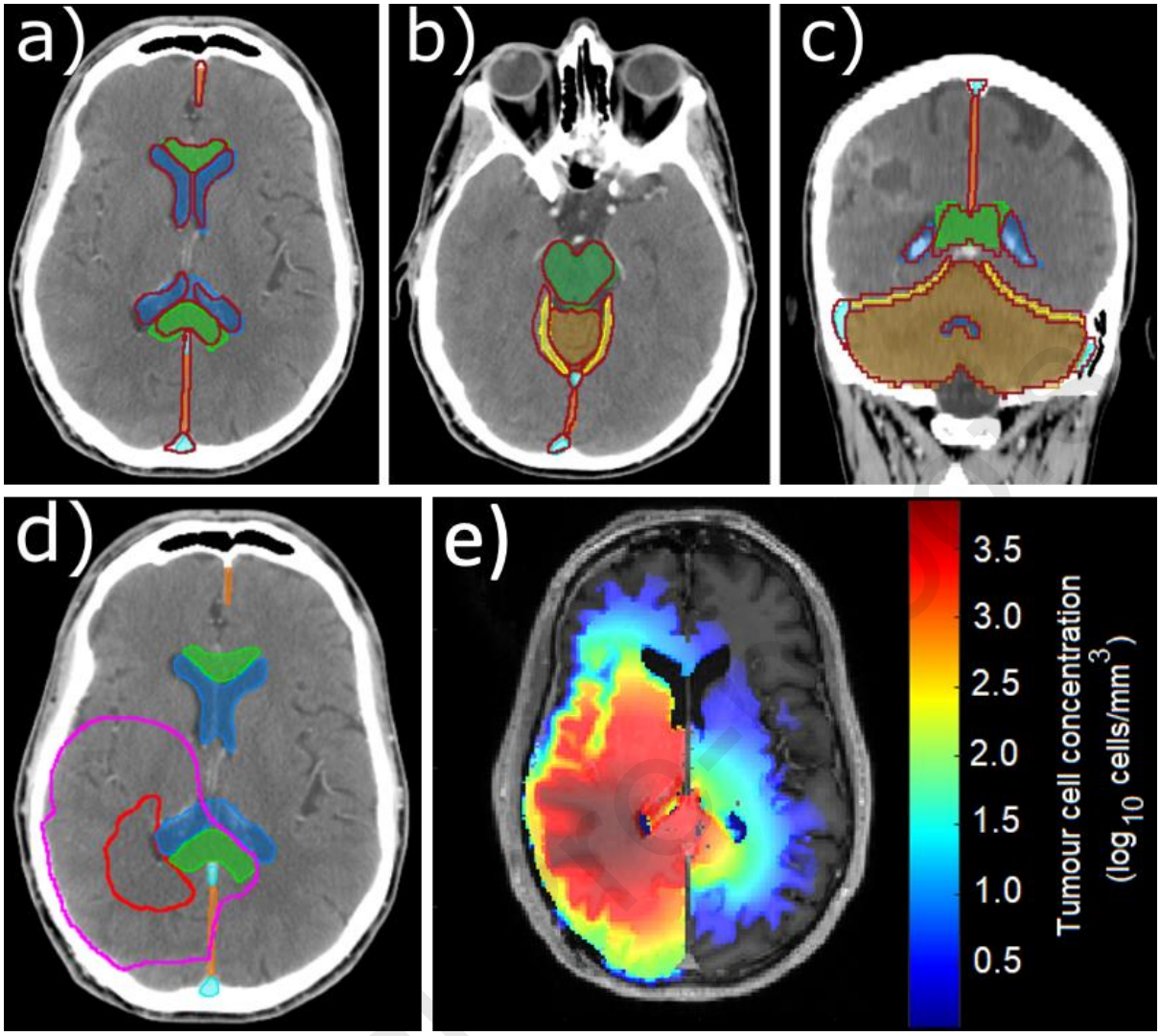
a)
b)
c)
d)
e)
3.5
3.0
2.5
2.0
1.5
1.0
0.5
Tumour cell concentration
(log10 cells/mm3)

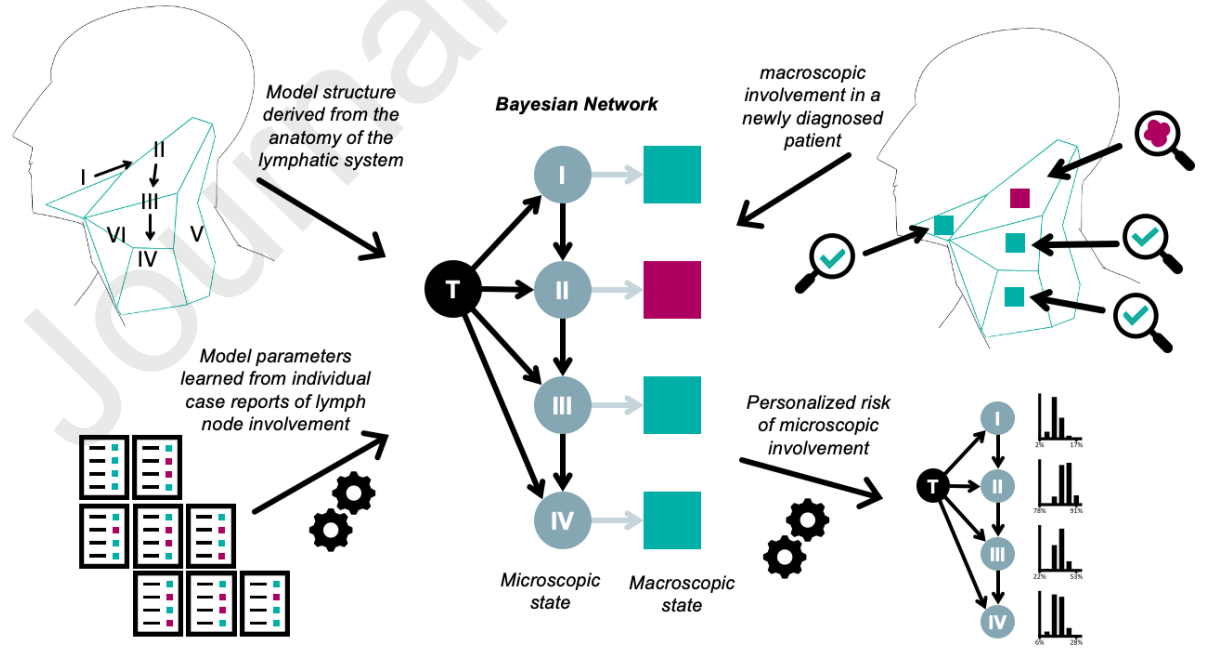
Model structure derived from the anatomy of the lymphatic system
I
II
III
IV
V
VI
Model parameters learned from individual case reports of lymph node involvement
Bayesian Network
T
I
II
III
IV
Microscopic state
Macroscopic state
macroscopic involvement in a newly diagnosed patient
Personalized risk of microscopic involvement

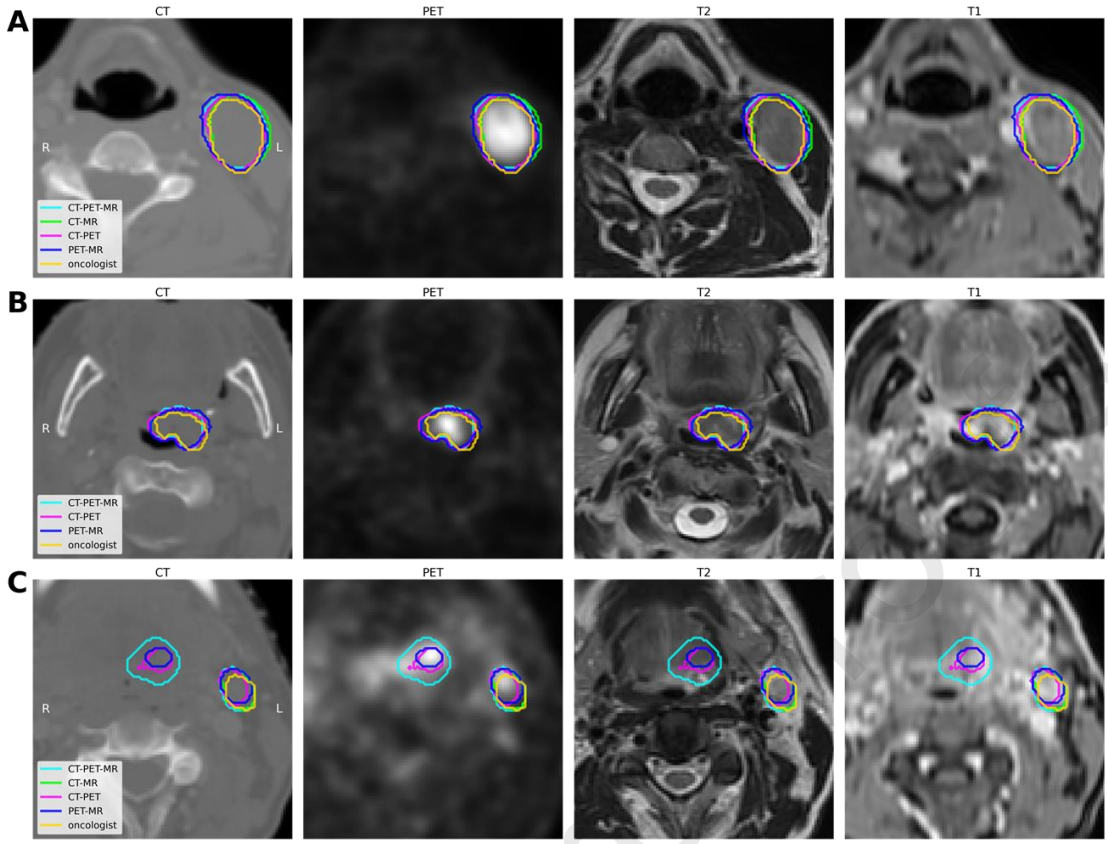

Table 1: microscopic tumor extension for head & neck SCC and NSCLC

Tumor location / Authors	# pts	tumor subsite / histology	Microscopic extension			
			Mean (mm)	Median (mm)	95% percentile (mm)	Maximum extension (mm)
Head & Neck SCC						
Ho (1997)	42	HYPO		-	< 10	25
Campbell (2012)	10	OC		0.99	3.95	7.8
Fleury (2014)	15	OC, ORO, HYP, LAR		1	5	15
Ligtenberg (2017)	25	LAR, HYPO		2.3	6.3	12.3
NSCLC						
Giraud (2000)	70	ADC SCC	2.69 1.48		8 6	
Li (2003)	43	ADC SCC	2.18 1.33		7 5	
Grills (2007)	71§	ADC	7.2		13#	
Van Loon (2012)	34	ADC + SCC	-		26*	

Abbreviations: LAR: larynx; HYPO: hypopharynx; NSCLC: non-small-cell lung carcinoma; OC: oral cavity; ORO: oropharynx; ADC: adenocarcinoma; SCC: squamous cell carcinoma;

§ T1-N0 only

based on GTV defined on the pathologic specimen

* 90% percentile

Highlights:

- Clinical target volume definition in radiotherapy is challenging
- The contribution of computational methods is discussed
- Goals are automation, consistency, and ultimately improvements
- Image segmentation algorithms can automate the process in parts
- Mathematical models may quantitatively describe tumor progression patterns

Conflicts of interest:

none